ADSORPTION OF As(III) FROM AQUEOUS SOLUTION ONTO IRON IMPREGNATED USED TEA ACTIVATED CARBON: EQUILIBRIUM, KINETIC AND THERMODYNAMIC STUDY

TAHIRA MAHMOOD[a], MADEEHA ASLAM[a], ABDUL NAEEM[a], TAHIR SIDDIQUE[b], SALAH UD. DIN[a]*

[a]*National Centre of Excellence in Physical Chemistry, University of Peshawar, Peshawar, Pakistan-25120*
[b]*Department of Applied Sciences, National Textile University Faisalabad, Pakistan-25120*

ABSTRACT

An efficient and cost effective adsorbent, activated carbon (UTAC) derived from used tea (UT) for the removal of As(III) from aqueous solutions was developed. To increase adsorption, UTAC was then impregnated with (magnetite) iron oxide particles (Fe-UTAC). The prepared adsorbents were characterized by XRD, SEM/EDX, FTIR and surface area analyzer. A comprehensive kinetic study of arsenite adsorption onto Fe-UTAC was conducted at 298-318 K and pH 8. The Richenberg model confirmed film diffusion to be the main rate limiting step. The removal of As(III) from aqueous solution onto Fe-UTAC was carried out as a function of temperature, concentration and pH. The sorption capacity (mol g^{-1}) of Fe-UTAC was observed to increase with increase in arsenite concentration while a decrease in the As(III) uptake was observed by increasing the temperature of the system. The sorption capacity of Fe-UTAC was almost three and six times larger than that of UTAC and UT respectively. The effect of pH on the arsenite adsorption was significant in the pH range 7–8 which may be correlated with the stability of Fe-UTAC as no release of iron from Fe-UTAC was observed. The mean free energy calculated from DR mechanism confirmed adsorption to be chemisorption and followed ligand exchange mechanism. The thermodynamic parameters confirmed adsorption to be exothermic, spontaneous and favorable.

Keywords: As(III); Used Tea; Iron Oxide; Anion exchange; Sorption.

1. INTRODUCTION

Arsenic industrialization has resulted in the release of large amounts of heavy metals such as copper, zinc, cadmium, arsenic, mercury, lead, nickel and chromium into water. These heavy metals are highly toxic, non-biodegradable and are a serious threat to mankind [1, 2].

Arsenic due to its mobility and high toxicity is considered to be one of the most hazardous contaminant and arsenic pollution has been declared a priority issue by the World Health Organization (WHO). It is found in the atmosphere, natural waters, soils as well as rocks. Both natural and anthropogenic sources are responsible for the discharge of arsenic into the environment. The natural processes involved in the distribution of arsenic are weathering reactions, volcanic emissions and biological activities while the anthropogenic sources are smelting of metal ores, use of arsenical insecticides, fertilizers, wood preservatives, electronics, glass and ceramic manufacturing industries [3, 4].

Arsenic exists in organic as well as inorganic forms**.** Inorganic As is more toxic than organic and exists as arsenite [As(III)] and arsenate [As(V)]. As(III) is estimated to be 25 - 60 times more toxic than As(V) [5]. At natural pH, arsenite [As(III)] exists as H_3AsO_3 and $H_2AsO_3^-$ and arsenate [As(V)] as H_3AsO_4, $H_2AsO_4^-$, $HAsO_4^-$ and AsO_4^{3-}. As(V) is dominant and stable under oxidizing conditions, while As(III) predominates under reducing conditions [6].

The most common pathway for human exposure to arsenic is through drinking water. The toxicity of arsenic is mostly due to its ability to interact with sulphydryl groups of the proteins and enzymes and thus stop the action of thiol group of enzymes [7]. As it causes toxic effects at low concentrations, the US Environmental Protection Agency (USEPA) has recently reduced the maximum contaminant limit (MCL) standard from 50 to 10 µg L^{-1}, which is also the WHO drinking water quality guideline for arsenic [8].

Arsenic is carcinogenic and its long term exposure causes cancer of lungs, kidneys, liver, and skin. Generally, acute and chronic poisoning causes skin lesions, loss of appetite, muscular weakness, diabetes, gastrointestinal and cardiovascular diseases [9, 10]. Naturally occurring arsenic in drinking water threatens the health and lives of people in many countries including Argentina, Chile, Mexico, China, Taiwan, Ghana, Hungary, Greece, Bangladesh, Vietnam, Poland, Canada, Japan, India, Iran and even in Pakistan [11, 12].

Arsenic removal from ground water is a challenging task due to large variation in physiochemical forms at different conditions. Presently, numerous techniques such as ion exchange, membrane separation, precipitation-coagulation, oxidation, reverse osmosis, nanofiltration and adsorption have been proposed to remove arsenic from water [13, 14]. However, the adsorption technique appears to be the most applicable because it is cost effective, easy to handle, versatile and has the ability to regenerate the adsorbent for re-use [15].

Several adsorbents such as oxides (iron oxides, manganese oxide, titanium dioxide, clay, activated alumina, zirconium oxide, mixed oxides etc.), hydroxides (iron hydroxide, aluminium hydroxide, lanthanum hydroxide etc.), metal phosphates (iron phosphate etc.), agricultural and industrial wastes (rice husk, pecan nut shell, sugarcane bagasse, tea waste, hazelnut and coconut shell, peels of various fruits, calcined bauxite, red mud etc.), polymer resins (Amberlite IRC-718, amberlite XAD-7, PolyHIPE etc.), biosorbents (coconut shell, mango leaf, orange peel, rice polish, banana peel etc.) and activated carbon (AC) have been tested by different researchers for the removal of arsenic from aqueous solution [3, 6, 8, 16].

AC has been recognized as an effective adsorbent due to its high surface area, highly developed porosity, large adsorption capacity, high surface reactivity and relative ease of regeneration [17]. However, one of the limitations in the use of commercial AC is its high cost. High demand for activated carbon has necessitated the search for new precursors as well as environmentally friendly methods for the production of activated carbon materials.

Attempts have also been made to develop activated carbon from cheaper and abundantly available materials using natural materials as well as agricultural and industrial wastes. AC can be synthesized by physical or chemical methods [18]. For lignocellulosic materials, $ZnCl_2$ and H_3PO_4 are commonly used as activating agents to produce activated carbon of high surface area. However, H_3PO_4 is preferred and widely used because of lower temperature required for activation, and to avoid problems of corrosion, inefficient chemical recovery and environmental disadvantages associated with $ZnCl_2$ [17, 19]. Usually, H_3PO_4 acts as a dehydrating reagent, which can stimulate decomposition of the cellulosic precursor at low temperature [20].

A variety of raw materials, namely pistachio-nut shell, guava seeds, peanut hulls, coconut shell, apricot stone, date pits, peach stone, coffee bean husks, chestnut wood, grape seed, corn cob, oat hulls, olive stone, rice husks and sugarcane bagasse have been exploited by researchers for the production of activated carbon [19-21].

Although the usefulness of activated carbons to act as adsorbent for many kinds of pollutants is well-known, but further research on activated carbon modification is gaining importance due to the need to enable activated carbons to enhance affinity for removal of various kinds of pollutants from waste water [22]. Iron oxides due to their low cost, non- toxicity and higher affinity for arsenic are mostly used for modification of activated carbon.

Recently, magnetic (Fe_3O_4) materials have attracted special attention in water treatment due to their strong adsorption affinities and the properties of being easily separated and reused by an external magnetic field [6].

In the present study, Black tea (Camellia sinensis leaves) is used as an adsorbent as it is the most popular and extensively used non-alcoholic beverage worldwide, after water. Pakistan is a major tea-consuming country, annually 240,000 tons of tea is consumed placing it as the seventh largest tea-consuming country in the world. It is consumed in thousands of tons every year and its proper disposal after use is a serious problem. The use of such environment friendly starting material may reduce solid waste pollution and also cost of raw material for the production of activated carbon.

Although activated carbon prepared from spent tea leaves, industry

e-mail: tahiramahmood@uop.edu.pk.

tea waste or tea waste biochar has been used for the adsorption of organic contaminants such as dyes, phenols and pesticides from aqueous solutions [23-25], however, it has not been tested for heavy metals particularly As(III). To the best of our knowledge, no former work has reported activated carbon from used tea (household) and iron oxide (magnetite) impregnated used tea activated carbon (Fe-UTAC) for the selective removal of As(III) ions.

The present work aims to investigate the possible use of tea waste (UT) for the biosorption of As(III) from aqueous solution. The main focus of this study is to develop activated carbon (UTAC) from abundantly available tea waste (UT) by chemical activation method using phosphoric acid and used as an adsorbent for the removal of As(III). Moreover, UTAC was impregnated with iron oxide (magnetite) particles to increase the adsorption capacity of As(III). The effect of various factors such as contact time, initial metal ion concentration, pH and temperature on adsorption were systematically examined. The sorption capacity of Fe-UTAC was tested and compared with various other sorbents already used for the removal of As(III). Further kinetic and thermodynamic studies have also been carried out.

2. EXPERIMENTAL DESIGN

2.1 Chemicals and reagents

Throughout the research work, all chemicals used were of analytical reagents grade and were used without further purification. Ferric chloride hexa hydrate, Ferrous sulphate hepta hydrate, Phosphoric acid, Hydrochloric acid, Nitric acid, Sodium hydroxide, Sodium Nitrate and Ammonium hydroxide were all purchased from Scharlau. All the stock and working solutions were prepared in distilled deionized water. Prior to the experiment, glassware used was first washed with tap water, followed by 10 % nitric acid solution and finally rinsed with deionized water. Arsenic standards for atomic absorption spectrophotometer were purchased from Scharlau Company.

2.2 Preparation of adsorbents

2.2.1 Preparation of Used tea (UT)

Used black tea (UT) of Lipton brand was collected from domestic source and boiled with deionized water at 80 °C for 1 h to remove its color, caffeine and tannins. It was further washed several times with double distilled water until colorless filtrate was obtained. It was then dried in an oven at 105 °C for 24 h. The dried material was crushed and sieved to 120 mesh size.

2.2.2 Preparation of Used tea Activated Carbon (UTAC)

Used tea activated carbon (UTAC) was prepared by chemical activation method in a tube furnace (TF 55030C-1 Thermoelectron Corporation, USA) at 500 °C using phosphoric acid (85 %) as an activating agent. UT was mixed with phosphoric acid (85 %) in a ratio of (1:1 w/v) and allowed to soak for 24 hours at room temperature. The impregnated mixture was then activated by placing in a quartz tube in tube furnace in the presence of nitrogen. The temperature of the tube furnace was first maintained at 170 °C under nitrogen flow rate of 100 ml min^{-1} for 1 hour. Then increased the temperature to 500 °C and the sample was held for 2 hours. Once the activation was completed, oven was switched off and carbonized material was then allowed to cool down to room temperature under nitrogen flow. The prepared UTAC was washed with deionized water in a soxhlet extractor at 100 °C, until the residual acid was removed and no phosphate ions were observed. The resulting UTAC was dried in oven at 105 °C for 24 hours and then stored in air tight bottle. The schematic procedure for the preparation of UTAC is shown in Fig. 1a.

2.2.3 Modification of Activated Carbon (Fe-UTAC)

Modification of the UTAC was carried out by impregnating with iron oxide (Fe_3O_4) fine particles. Synthesis of magnetite fine particles (Fe_3O_4) was carried out by homogenous precipitation method reported by Panneerselvam [26]. For this process, 3.1 g of $FeCl_3 .6H_2O$ and 2.1 g of $FeSO_4.7H_2O$ were dissolved in 80 mL of deionized water under inert atmosphere with vigorous stirring. Solution was heated to 80 °C, when the required temperature was achieved; 10 mL of NH_4OH solution (25 %) was drop wise added to obtain the formation of black precipitates of Fe_3O_4 fine particles. These were then mixed with 10 g of adsorbent (UTAC) and heated at 80 °C for half an hour under vigorous stirring. The resulting suspension was cooled down to room temperature and then washed several times with deionized water to remove impurities**.** The schematic procedure for the preparation of UTAC is shown in Fig. 1b and the reaction involved during impregnation of UTAC is represented by equation 2.

$$FeSO_4 \cdot 7H_2O + 2FeCl_3 \cdot 6H_2O + 8NH_4OH \longrightarrow Fe_3O_4 + 6NH_4Cl + (NH_4)_2SO_4 + 17H_2O \quad (1)$$

$$Fe_3O_4 + UTAC \longrightarrow UTAC\text{-}Fe_3O_4 \quad (2)$$

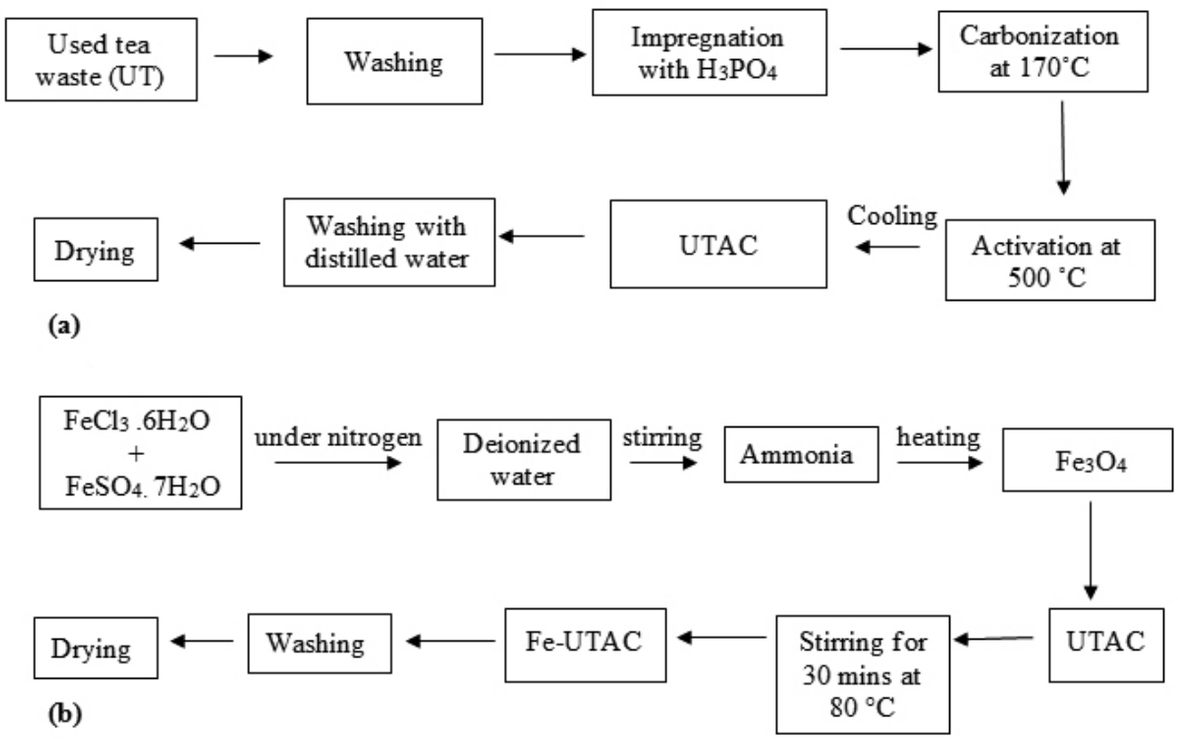

Fig. 1. Schematic diagram of UTAC and (b) Fe-UTAC Preparation**.**

The iron oxide impregnated used tea activated carbon (UTAC-Fe_3O_4) was dried in an oven for 24 hours at 110 °C and will be onwards referred to as Fe-UTAC.

2.3 Characterization

The characterization of UT, UTAC and Fe-UTAC was carried out using various analytical techniques. Surface areas (S_{BET}) of the samples were determined using a surface area analyzer (Quantachrome NOVA 1200e) by nitrogen adsorption/desorption method. The morphologies of adsorbents were examined by scanning electron microscopy (SEM; JSM-6490, JEOL) at 20 keV and elemental composition of the adsorbents was determined by energy dispersive X-ray analyzer (EDX Inca-200). FTIR analyses of the adsorbents were carried out using an infrared spectrophotometer (Shimadzu 8201PC) in the wavelength range of 400 – 4000 cm^{-1}. The X-ray diffraction patterns of the samples were recorded using JEOL X-ray diffractometer (model JDX-3532) with Mn filtered Cu-Kα radiations in the 2θ ranging from 10 - 80°. To determine the stability of Fe-UTAC, a known amount (0.1 g) of the adsorbent in 40 mL $NaNO_3$ solution was equilibrated for 24 h at different pH values. After equilibration the aqueous filtrates were analyzed for the release of Fe from the Fe-UTAC.

2.4 Adsorption studies

Batch adsorption experiments were conducted to examine the effect of concentration, pH and temperature on the sorption of As(III) (Scharlau) onto Fe-UTAC. The working solutions of arsenite were prepared from 1000 mg L^{-1} standard solution of As(III). For each experiment, 0.1 g of the adsorbent was added to 40 ml of As(III) solution of different concentrations (5 - 100 mg L^{-1}). The initial pH of each solution was adjusted to 8 using either hydrochloric acid or sodium hydroxide solution. The samples were placed in shaker bath [model DAIHAN WSB-30 (Korea)] at a shaking speed of 120 rpm at 298 K for 24 hrs. After equilibration, the final pH of each solution was noted. All the solutions were then filtered and the filtrates were analyzed for As(III) and iron released from the iron impregnated activated carbon using atomic absorption spectrophotometer (AAS 800). The amount of As(III) adsorbed (X) was determined from the difference of the initial and the equilibrium concentration of the As(III) in aqueous solution by using the following expression:

$$X = \frac{V\,(C_i - C_e)}{1000m} \quad (3)$$

Where V refers to the volume of the solution (mL), m is the mass of the adsorbent (g) and C_i and C_e are the initial and equilibrium concentrations (mol L^{-1}) of the As(III) respectively. Adsorption studies of arsenite onto UT and UTAC were also conducted for comparison with Fe-UTAC at pH 8 and 298 K.

The effect of pH on the removal of As(III) by Fe-UTAC was examined at various pH values (3-12) at 298 K with different concentrations of As(III) solutions. Temperature studies were carried out at 298, 308, 318 and 328 K at pH 8 with different concentrations of As(III) solutions.

Adsorption kinetics experiments for 25 mg L^{-1}As(III) were carried out at pH 8 at different temperatures (298-318 K) and various time intervals (5 min to 24 h).

3. RESULTS AND DISCUSSION

3.1 Characterization

3.1.1 Surface area and pore size distribution

The Brunaeur-Emmett and Teller (BET) surface areas of UT, UTAC and Fe-UTAC are given in Table 1. The BET surface area for the UTAC prepared by chemical activation with phosphoric acid was found to be 243 m^2g^{-1}, which is in good agreement with the values reported in literature under same conditions [27-29]. However, activated carbon produced in our study showed higher BET surface area than tea or lignocellulosic materials already reported in literature [24, 25, 30, 31]. The BET surface area of Fe-UTAC was 165 m^2 g^{-1}. This decrease in surface area can be attributed to the covering of UTAC surface by iron oxide particles during impregnation which was also confirmed later by the SEM results. Decrease in surface area was also observed by Nethaji et al. [29] while impregnating corncob activated carbon (CCAC) with magnetic nanoparticles. Similarly, Maiti et al. [32] also observed decrease in surface area by impregnating tarmarind hull carbon (THC) with iron oxide.

The pore diameter and pore volume of UTAC were found to be 123 Å and 0.47 cc g^{-1} respectively. These values decrease to 35 Å and 0.16 cc $g^{-1}$for Fe-UTAC. The decrease in pore diameter has also been reported by Mohan et al. [33] for the development of activated carbon from almond shells. The average pore diameters of all the adsorbents lie in the range of 20 – 500 Å. This pore size distribution (PSD) suggests that the adsorbents used in this study are mesoporous in nature.

Table 1. Surface area, pore size distribution and elemental composition of UT, UTAC and Fe- UTAC.

Adsorbent	Surface Area [m^2 g^{-1}]	Pore Diameter [Å]	Pore Volume [cc g^{-1}]	Elemental composition % weight					
				C	O	B	Ca	P	Fe
UT	80	118.5	1.68	63	12	23	0.7	–	–
UTAC	243	123.4	0.47	89	9.2	–	–	1.7	–
Fe-UTAC	167	35.8	0.16	55	13	–	–	0.7	37

3.1.2 SEM/EDX studies

The SEM images (Fig. 2 a-c) illustrate the porous nature and irregular morphology of UT, UTAC and Fe-UTAC. The decrease in porosity in the case of Fe-UTAC as compared to its precursor UTAC is most probably due to the blockage of pores of UTAC by iron oxide particles [34]. Thus, it is suggested that impregnation of UTAC by the iron oxide has been done effectively. Liu et al. [34] observed similar morphology and decrease in porosity for waste material derived activated carbon after Fe_3O_4 loading.

Energy dispersive X-ray spectroscopy (EDX) of the samples were carried out for elemental analysis. EDX spectra of UT, UTAC and Fe-UTAC are presented in Fig. 2 (d-f) respectively and data in Table 1. EDX data of UT showed weight% composition of carbon, boron, oxygen and calcium to be 63, 23, 12 and 0.7 respectively. The presence of *Boron in tea samples has already been reported by Krejcova and Tomas [35] where it has been mentioned that it is a beneficial element for humans, plants and animals.* The EDX data of UTAC showed carbon 89 %, oxygen 9.2 % and phosphorous 1.7 % by weight. While Fe-UTAC consists of carbon (55.3%), oxygen (13%), phosphorous (0.7%) and iron (31%). EDX of Fe-UTAC signified a considerable amount of Fe in the sample, thus suggesting the presence of iron in Fe-UTAC which strongly supports the impregnation of UTAC with iron oxide.

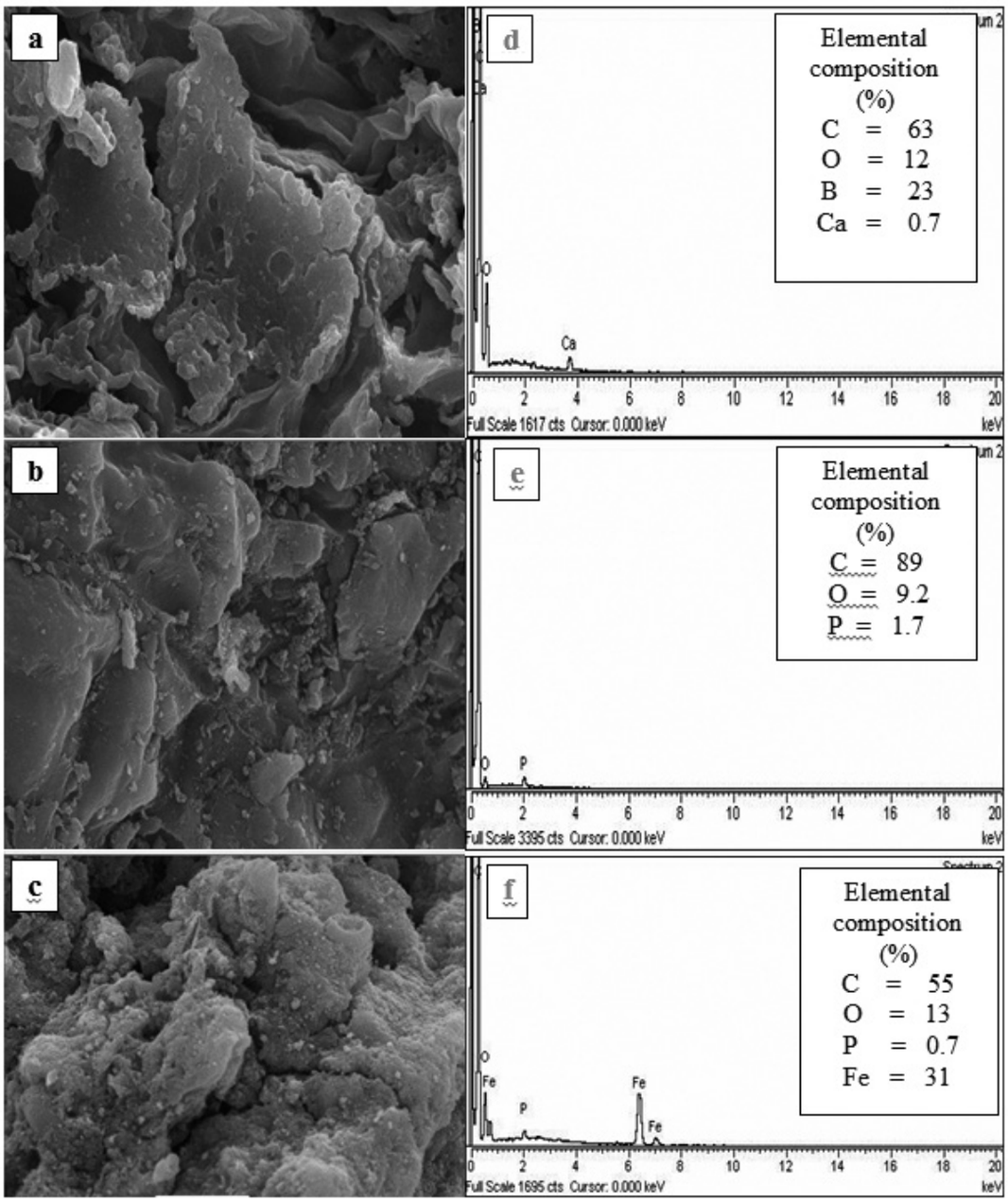

Fig. 2. SEM (a, b, c) / EDX (d, e, f) of UT, UTAC and Fe-UTAC.

3.1.3 FTIR studies

The IR spectra of UT, UTAC and Fe-UTAC are given in Fig. 3 (a-c). The IR spectrum of UT shows a number of absorption peaks, signifying the intricate nature of adsorbent. A broad band was observed at 3342 cm^{-1}, which was assigned to –OH group, while the weak bands observed at about 2931 and 2852 cm^{-1} were ascribed to the C–H stretching. Similarly, the bands observed at 1523 and 1457 cm^{-1} correspond to secondary amine group and symmetric bending of CH_3 as reported by Malkoc and Nuhoglu [36]. The peak observed at 1646 cm^{-1} was due to C═O stretching, while the small peaks appeared at 1234 and 1049 cm^{-1} could be assigned to $–SO_3$ and –C–C group respectively as reported by Panneerselvam et al. [27] for magnetic nano particles impregnated onto tea waste.

The spectra of UTAC and Fe-UTAC are almost similar. The spectra shows strong absorption band at 3481 cm^{-1}, this band can be assigned to the O–H stretching mode of hydroxyl groups and adsorbed water. While the weak band observed at about 3057 cm^{-1} could be ascribed to the asymmetric C–H band. A small peak at 1692 cm^{-1} probably corresponded to the stretching vibration of C═O in carboxylic acid and quinine type structure as reported by Marin et al. [37]. Similarly, bands at 1594 and 1447 cm^{-1} were the skeletal C═C vibrations of aromatic rings as reported by Liou [38]. The peaks at 1215 and 1069 cm^{-1} were assigned to P═O bond. Furthermore, the appearance of a new band at 583 cm^{-1} in the case of Fe-UTAC was assigned to the stretching and torsional vibration of Fe–O. Similar results have been reported by Liu et al. [34] and Karaagac et al. [39].

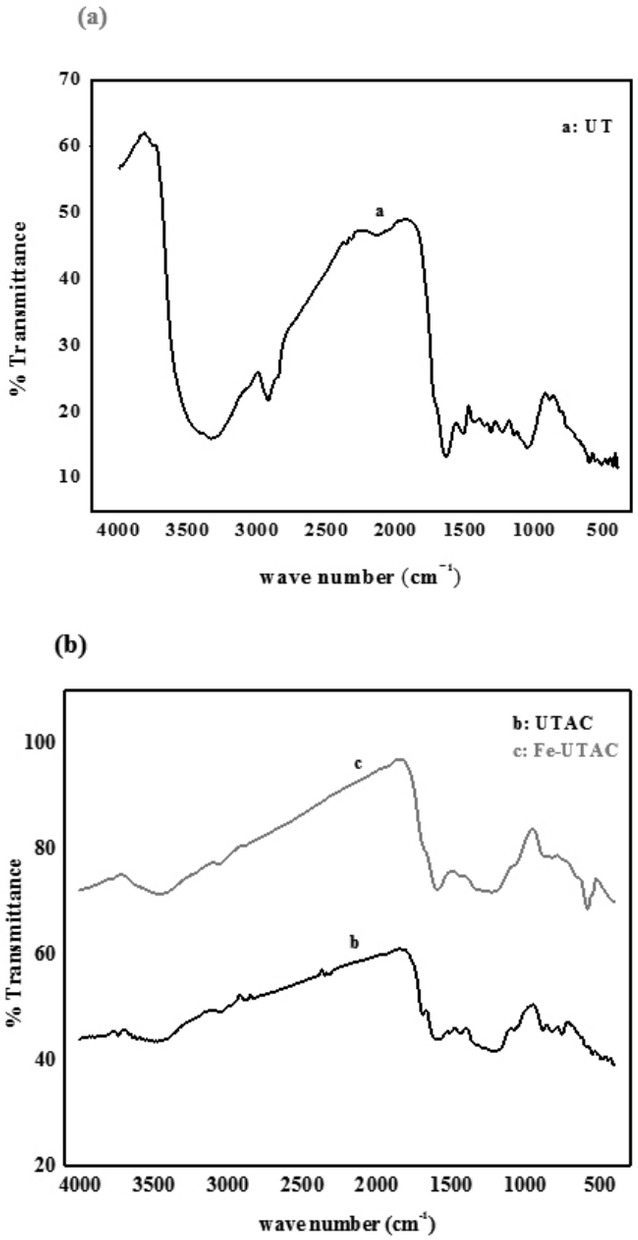

Fig. 3. FTIR spectra of (**a**) UT (**b**) UTAC and Fe-UTAC.

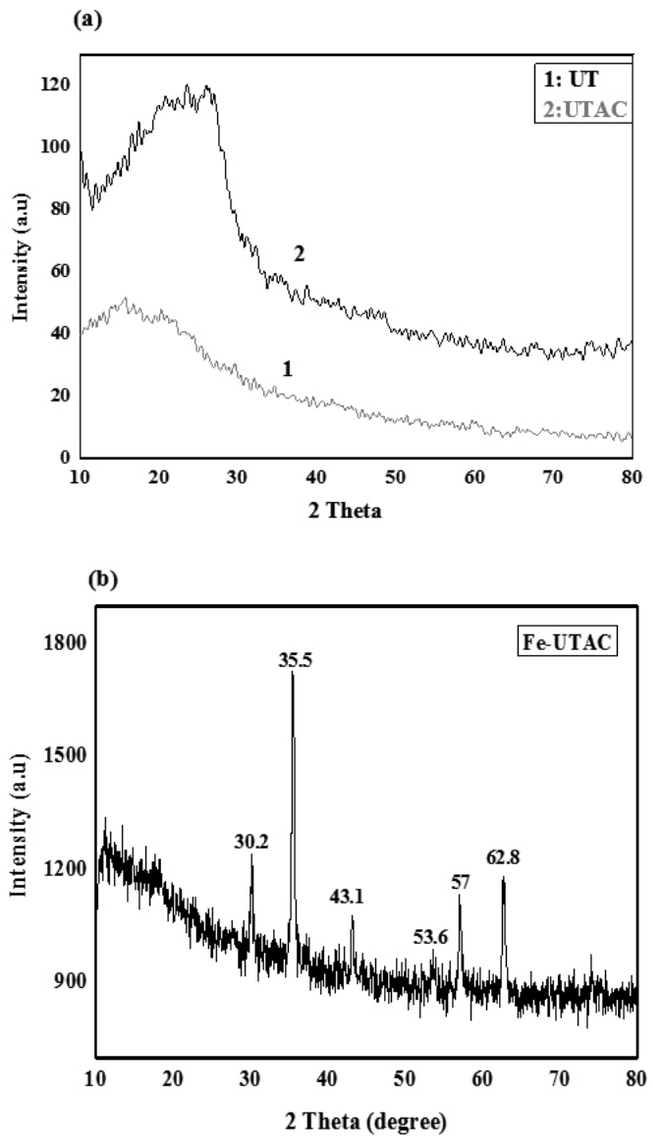

Fig. 4. XRD pattern of (**a**) UT and UTAC (**b**) Fe-UTAC

3.1.4 XRD studies

The XRD spectra of UT and UTAC (Fig. 4 a) indicated their amorphous nature. However, the XRD pattern of Fe-UTAC (Fig. 4 b) showed that it is crystalline, having peaks at 2θ (30.2°, 35.5°, 43.1°, 53.6°, 57° and 62.8°) which are the characteristic peaks of inverse-spinel structure of Fe_3O_4 matching with JCPDS (card No. 85-1436). This indicated that impregnation with iron oxide has been done effectively resulting in crystalline Fe-UTAC. These results are consistent with those reported in literature for magnetite (Fe_3O_4) impregnated activated carbon [34, 40].The crystallite size was calculated to be 12 nm using the Debye-Scherrer equation.

$$d = \frac{k\lambda}{\beta\cos\theta} \quad (4)$$

where k is the Debye- Scherrer constant (0.89), β is the full width at half maximum, λ is the wavelength (1.54 A°) and θ, the Bragg angle.

Detailed adsorption and kinetics studies were carried out for the adsorption of As(III) onto Fe-UTAC to probe into the mechanism of the adsorption process.

3.2 Adsorption kinetics

The kinetics of As(III) adsorption onto Fe-UTAC was studied to investigate the sorption behaviour of the system. The adsorption of As(III) on Fe-UTAC at different time intervals (5 min - 24 h) and pH 8 is shown in Fig. 5. The figure shows a rapid uptake of As(III) in the first 150 min, followed by a steady and slower uptake until an equilibrium is attained in 3 h. The rapid uptake of As(III) in the beginning can be attributed to the presence of a large number of vacant sites on the surface of Fe-UTAC. However, the adsorbent surface gets saturated after certain time period, equilibrium is established in the system and no further sorption of As(III) occurs. It is obvious from the figure that the adsorption curves of arsenite are smooth and continuous leading to saturation, suggesting the probability of monolayer coverage of the surface. Similar equilibrium time for As(III) adsorption by fly ash has been reported by Polowczyk et al. [9].

Temperature has a significant effect on the kinetics of arsenite sorption onto Fe-UTAC, and the uptake of arsenite decreases with the rise of temperature from 298 - 318 K (Fig. 5). The decrease in arsenite sorption with increase in temperature indicates that the sorption process is exothermic. However, the equilibrium time for the arsenite sorption remained the same with an increase

in temperature and thus is independent of temperature. Similar behavior of arsenite sorption has been reported by Podder and Majumder [41].

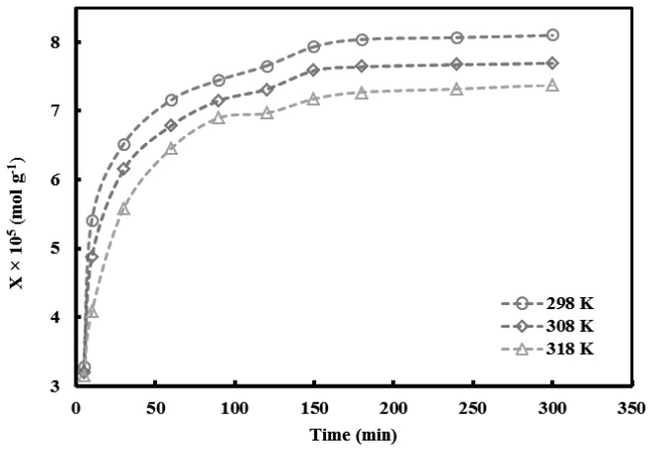

Fig. 5. Effect of time on As(III) adsorption onto Fe-UTAC at pH 8.

3.3 Kinetic modeling

In order to explain the kinetics mechanism for the As(III) adsorption on Fe-UTAC, different kinetics models such as pseudo-first order, pseudo second-order, Elovich, Weber Morris and Richenberg models were applied to the current data.

3.3.1 Pseudo first order model

The linear form of pseudo first order kinetic model is given as:

$$ln(X_e - X_t) = ln X_e - k_1 t \quad (5)$$

where X_t is the amount adsorbed at time t, X_e is the amount adsorbed at equilibrium time and k_1 is the rate constant. By plotting ln (X_e - X_t) vs. t, straight lines were obtained and are shown in Fig. 6a. The amount adsorbed (X_e) and rate constant (k_1) were calculated from intercepts and slopes of the plots and are summarized in Table 2. The pseudo first order model failed to explain the current data due to the poor R^2 values and difference between experimental and theoretical values. Similar results have been reported by Mahmood et al. [42] for arsenate adsorption onto iron hydroxide.

3.3.2 Pseudo second order model

The pseudo second-order kinetic model in its linear form is given as:

$$\frac{t}{X_t} = \frac{1}{k_2 X_e^2} + \frac{1}{X_e} t \quad (6)$$

where X_e and X_t is the amount of arsenite adsorbed at equilibrium and at time t respectively and k_2 is the second order rate constant. A straight line was obtained from the plot of t/X_t vs. t with $R^2 > 0.99$ (Fig. 6b). The values of rate constant (k_2) and amount adsorbed (X_e) were calculated from intercept and slope respectively (Table 2). The amount of As(III) adsorbed (X_e) calculated theoretically from the pseudo second order model is comparable in magnitude with its experimental value. This suggests that the current experimental data follow the pseudo second order model. A similar decrease in the rate constant values with increase in temperature has been reported by Ranjan et al. [43] for biosorption of arsenite using agricultural residue rice polish.

Both the k_2 and X_e values decrease with increase in temperature, which indicates the exothermic nature of the process. The application of pseudo second order equation suggests that chemisorption is the possible route of As(III) sorption onto Fe-UTAC.

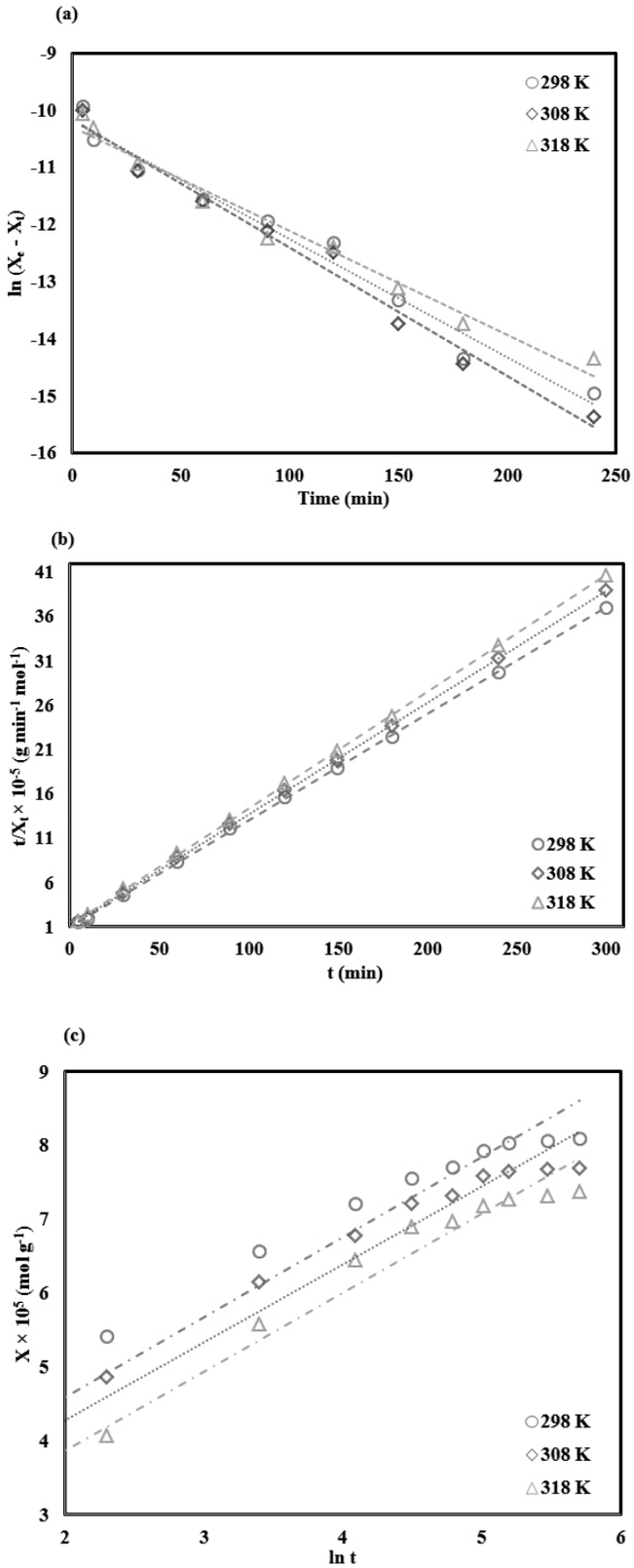

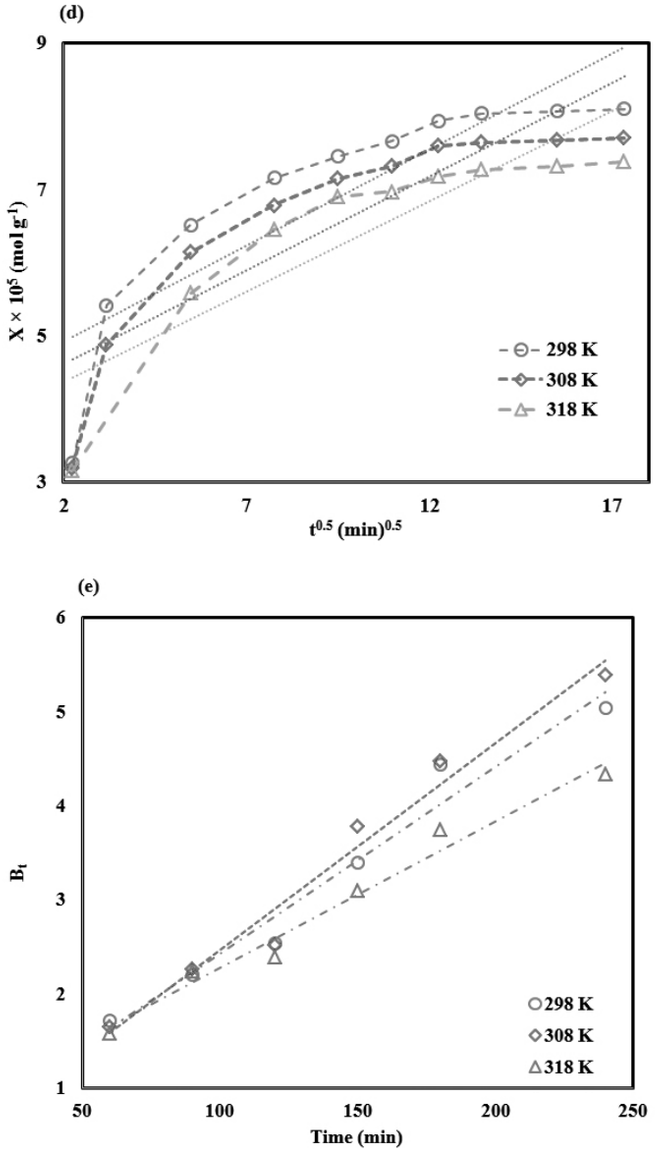

Fig. 6(**a**) Pseudo first order, (**b**) Pseudo second order, (**c**) Elovich, (**d**) Weber Morris and (**e**) Richenberg plots for As(III) sorption onto Fe-UTAC.

3.3.3 Elovich Model

The Elovich equation can be written in the following form:

$$X = \frac{\ln(\alpha ß)}{\beta} + \frac{lnt}{\beta} \quad (7)$$

where α and β are constants representing the rate of chemisorption at zero coverage and the extent of surface coverage and activation energy for chemisorption. These constants were calculated from the intercept and slope of the plots of X vs. ln t (Fig. 6c) which showed good linear relationships with R^2 values greater than 0.9 at all temperatures and are represented in Table 2. This suggests that the sorption of As(III) onto Fe-UTAC followed the pseudo-second-order kinetic model based on the assumption that chemisorption may be the rate determining step.

3.3.4 Weber and Morris model

The Weber Morris model was applied to the kinetic data to explore the possibility of intraparticle diffusion as the rate limiting step. It is an empirical equation and can be mathematically written as:

$$X = k_{id} t^{0.5} + C \quad (8)$$

where C is the intercept, a constant representing boundary layer effect and k_{id} (mol g^{-1} $min^{-0.5}$) is the intraparticle diffusion rate constant obtained from slope of plots of X vs. $t^{0.5}$ (Fig. 6d). The values of k_{id} at different temperatures are given in Table 2.

The larger the value of C, the greater is the boundary layer effect. If the plot of X vs. $t^{0.5}$ is linear and passes through the origin with no intercept, intraparticle diffusion is the rate determining step. In the present study, linear plots of X vs. $t^{0.5}$ do not pass through the origin, which means that intraparticle diffusion is not the only rate determining step. The adsorption process may be controlled by more than one mechanism with the initial curved portions of the plots (Fig. 6d) suggesting film diffusion (boundary layer) and the linear portions representing intraparticle diffusion. The present findings are in agreement with the data reported in literature [42].

Table 2. Kinetic parameters for As(III) adsorption on Fe-UTAC at pH 8 and different temperatures.

Parameters	Temperature [K]		
Models	298	308	318
Pseudo first order $X_e \times 10^5$ [mol g^{-1}] Exp $X_e \times 10^5$ [mol g^{-1}]Theo $k_1 \times 10^3$ [min^{-1}] R^2	8.09 3.78 20 0.97	7.69 3.91 22 0.98	7.37 3.37 18 0.97
Pseudo second order $X_e \times 10^5$ [mol g^{-1}] Exp $X_e \times 10^5$ [mol g^{-1}]Theo $k_2 \times 10^{-3}$[g $min^{-1}mol^{-1}$] R^2	8.09 8.32 1.47 0.999	7.69 7.94 1.44 0.999	7.37 7.60 1.41 0.999
Elovich $\alpha \times 10^{-5}$[mol g^{-1} min^{-1}] $\beta \times 10^5$ [g mol^{-1}] R^2	6.18 1.14 0.93	5.43 1.11 0.95	3.58 1.12 0.98
Weber-Morris $K_{id} \times 10^6$ [mol $g^{-1}min^{-0.5}$] C R^2	2.63 4.39 0.75	2.56 4.10 0.77	2.47 3.87 0.76

3.3.5 Richenberg Model

The Richenberg model which differentiates between film and intraparticle diffusion and is given as follows:

$$F = 1 - \frac{6}{\pi^2} \sum_m^1 \frac{1}{m^2} exp(-m^2 B_t) \quad (9)$$

where F is the fractional attainment of equilibrium at time t, and is obtained by the following expression;

$$F = \frac{X_t}{X_e} \quad (10)$$

B_t is a mathematical function of X which can be evaluated from the equation given below:

F values > 0.85

$$B_t = -0.4977 - ln(1 - F) \quad (11)$$

and for

F values < 0.85

$$B_t = (\sqrt{\pi} - \sqrt{\pi - \frac{\pi^2 F}{3}})^2 \quad (12)$$

The plots of B_t vs. t at different temperatures are shown in Fig. 6e. If a plot of B_t vs. t is linear passing through the origin, then the rate determining step is particle diffusion, otherwise, it is followed by film diffusion. In the present study, the plots are straight lines, but do not pass through the origin. Hence, it is concluded that film diffusion is the main rate limiting step for the sorption of arsenite by Fe-UTAC.

3.4 Equilibrium adsorption studies

3.4.1 Effect of arsenite concentration and temperature

The effect of arsenite concentration on its adsorption onto UT, UTAC and Fe-UTAC at 298K is given in Fig. 7a. An increase in arsenite concentration led to increase in the adsorption capacities (mol g^{-1}) which may be due to the availability of more arsenite ions in solution. The probability of collision between arsenite ions and adsorbent increases, which results in the increased adsorption by all the three substrates. Comparison of the adsorption capacities of the adsorbents used in the present study shows that As(III) adsorption follows the order; Fe-UTAC >UTAC>UT. Arsenite adsorption by Fe-UTAC (9.11×10^{-5}mol g^{-1}) is almost 3 times greater than UTAC (2.79×10^{-5} mol g^{-1}) and 6 times than UT (1.43×10^{-5} mol g^{-1}). The higher adsorption capacity of Fe-UTAC as compared to UTAC and UT can be attributed to the higher affinity of iron oxide for As(III). Moreover, adsorption of arsenite by UTAC is almost double as compared to UT. The relatively greater uptake in case of UTAC than its precursor UT is due to its higher surface area (243 m^2 g^{-1}) than UT (80 m^2 g^{-1}). These results are comparable to those reported by Maiti et al. [33] for As(V) adsorption on iron oxide impregnated tamarind hull carbon (IOITHC) as compared to tamarind hull carbon (THC).

Arsenite adsorption onto Fe-UTAC was studied at 298 - 328 K. It is obvious from Fig. 7b that temperature has a significant effect on the As(III) adsorption by Fe-UTAC. The uptake of arsenite onto Fe-UTAC was found to be maximum at 298 K and minimum at 328 K. By increasing temperature, the attractive forces between adsorbent surface and metal ions are weakened and therefore sorption decreases. Thus, it is concluded that the decrease in sorption of arsenite on Fe-UTAC indicates that the adsorption phenomenon is exothermic in nature. Similar temperature effect has been reported by others in literature [41, 44, 45].

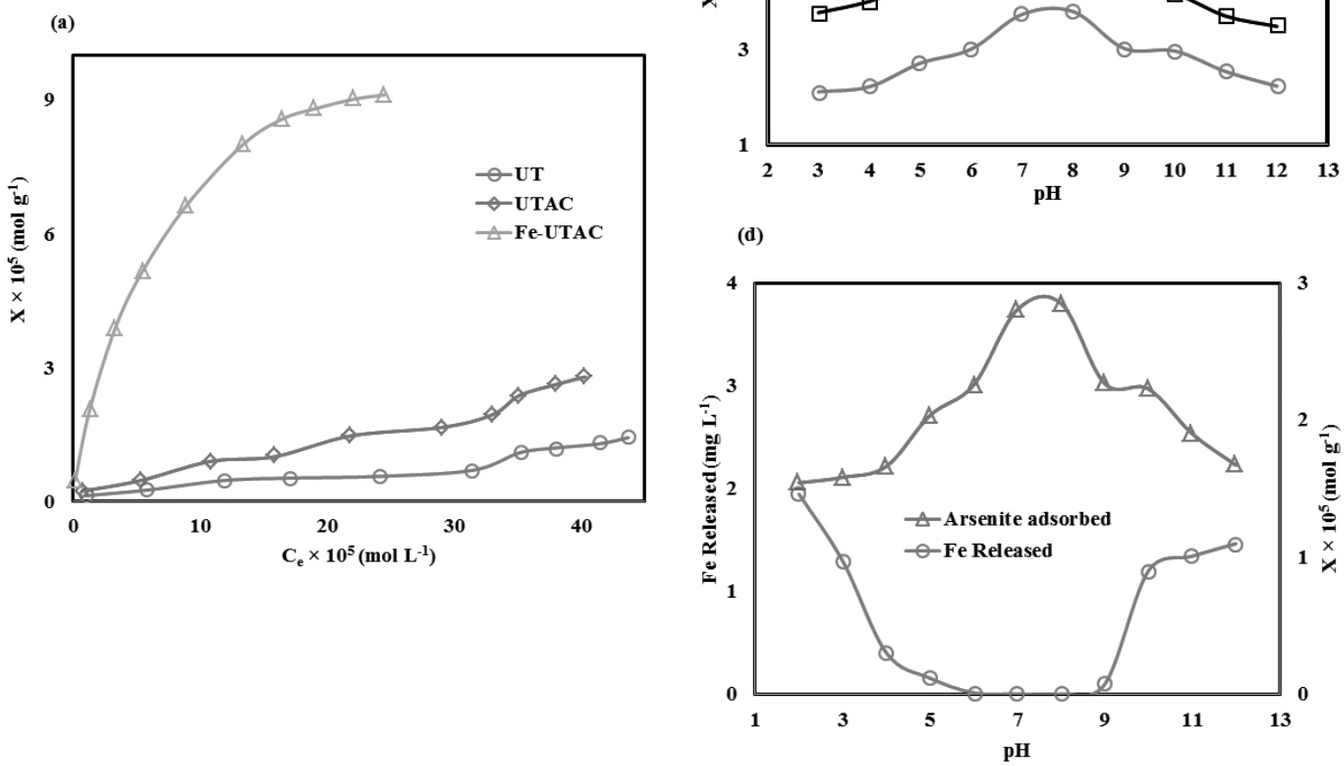

Fig. 7(**a**) Comparative adsorption affinity of arsenite towards adsorbents at pH 8 and at 298 K, (**b**) Effect of temperature, (**c**) pH effect on arsenite sorption onto Fe-UTAC at pH 8 and (**d**) Release of iron from Fe-UTAC and As(III) sorption at different pHs.

3.4.2 Effect of pH

The effect of pH on the adsorption of As(III) onto Fe-UTAC was studied in the range 3 – 12 at 298 K (Fig. 7c). As can be seen that the pH has a little effect on As(III) adsorption and maximum adsorption is observed at pH 7 and 8, however further increase in pH adsorption decreases. This adsorption behavior of arsenite at different pH may be due to the fact that As(III) exists in different oxyanionic forms. As(III) exists in non-ionic (H_3AsO_3) form below pH 7 and weak van der Waals forces most probably exist between H_3AsO_3 and the surface of Fe-UTAC. But as the pH approaches 7, a small percentage of H_3AsO_3 dissociates into anionic species ($H_2AsO_3^-$ and $HAsO_3^{2-}$) and higher arsenic uptake by Fe-UTAC is expected due to more specific binding [46]. The decrease in As(III) adsorption at pH 9 – 12 may be due to the electrostatic repulsions between $H_2AsO_3^-$ and $HAsO_3^{2-}$ and the negatively charged surface. Another reason for reduced adsorption may be the competition between hydroxyl ions and arsenite anions for the same sites on the adsorbent surface [47]. Maximum adsorption for As(III) at pH 7 has been reported by Podder and Majumder [41] onto granular activated carbon/$MnFe_2O_4$. Similarly, Tawabini et al. [48] reported maximum percent removal of As(III) at pH 7 and 8 and decrease in adsorption at pH 9 for iron oxide nanoparticles impregnated on carbon nanotubes. Moreover, Kocabas and Yurum [49] observed maximum adsorption of As(III) at pH 7.56 by Ferric ion loaded red mud.

It is suggested that Fe (III) is adsorbed on UTAC by releasing protons from the cellulose unit according to a cation exchange mechanism. Treatment with iron results in the production of adsorption sites of magnetite particles on the exterior surface of adsorbents. The adsorbed iron will coordinate with hydroxyl ions and neutral water molecules that are available in the aqueous medium.

The adsorption of arsenite on Fe-UTAC may be termed as a ligand exchange mechanism. Ligands involved in such exchange processes may be hydroxyl ions or neutral water molecules existing in the Fe-coordinated sphere. Thus, the adsorption of arsenite may take place by releasing a hydroxyl anion or neutral water molecules from its coordinated sphere and hence the following mechanism may be responsible for the adsorption of arsenite anions:

$$\equiv FeOH + H_3AsO_3 \Longrightarrow \equiv FeH_2AsO_3 + H_2O \quad (13)$$

$$\equiv 2[FeOH] + H_3AsO_3 \Longrightarrow \equiv FeHAsO_3Fe + 2H_2O \quad (14)$$

$$\equiv FeOH + H_2AsO_3^- \Longrightarrow \equiv FeHAsO_3^- + H_2O \quad (15)$$

$$\equiv 2[FeOH] + H_2AsO_3^- \Longrightarrow \equiv FeHAsO_3Fe + 2HO^- + H^+ \quad (16)$$

where ≡ FeOH refers to the solid surface of Fe-UTAC. Equations (13) and (15) represent adsorption of arsenite on the surface of Fe-UTAC through monodentate ligand exchange and equations (14) and (16) represent bidentate ligand exchange with hydroxyl groups.

As(III) removal at pH > 7 is due to the contribution of monovalent arsenite anion whose distribution is significant at this pH (eq.15 and 16). Whereas arsenite adsorption taking place at pH < 7 is due to the adsorption of neutral arsenite molecules accompanied by the release of water molecules according to the reaction mechanism (eq.13 and 14).

This mechanism is confirmed by its high value of free energy (E) i.e. 10 kJ mol^{-1} obtained from D-R isotherm that showed reaction is chemisorption in nature. The mechanism is further augmented by the fact that the pH of the solution had increased or almost no change had taken place after arsenic adsorption. Similar mechanism has also been suggested by Biswas et al. [50] for the removal of As(III) using Zr (IV) loaded orange waste. Ngantcha et al. [51] also reported ligand exchange mechanism for As(III) onto iron impregnated carbon.

It is important to mention here that no release of Fe from Fe-UTAC was detected in pH range 2 - 12 in the absence of As(III). However, in the presence of arsenite, a slight release of iron atoms from the Fe-UTAC was observed (Fig. 7d) in the pH range 2 - 3 and 10 - 12. The release of iron in the presence of As(III) indicates that the arsenite anion is dragging iron from the Fe-UTAC to form complexes in the aqueous phase. The maximum arsenite adsorption in the pH range 7 - 8 may therefore also be correlated with the stability of Fe-UTAC as no release of iron from Fe-UTAC was observed in this pH range.

3.5 Adsorption models

3.5.1 Langmuir model

The Langmuir model provides useful information regarding the maximum sorption capacity in the form of monolayer coverage. The linear form of the conventional Langmuir equation may be written as follows:

$$\frac{C_e}{X} = \frac{1}{K_b X_m} + \frac{C_e}{X_m} \quad (17)$$

where C_e and X are the amounts of arsenic in solution and at the solid surface respectively**.** The values of maximum sorption capacity (X_m) obtained from Langmuir isotherms (Fig. 8a) are comparable to the experimental values (Table 3). The values of binding energy constant (K_b) are sufficiently high, indicating that strong binding forces are involved in the sorption of arsenite onto Fe-UTAC. The values of X_m and K_b decrease with the rise of temperature (298 – 328 K), which indicate that the process of adsorption is exothermic in nature. This further augments the observation made in the adsorption isotherm (Fig. 7b) where the adsorption was found to decrease with increase in temperature. Similar decreasing trend for X_m and K_b values with increase in temperature was reported by Ranjan et al. [43].

Table 3. Langmuir, D-R and thermodynamics parameters for As(III) adsorption on Fe-UTAC at pH 8 and different temperatures.

Langmuir Parameters				D-R Parameters			Thermodynamics Parameters		
Temp [K]	$X_m \times 10^5$ [mol g^{-1}]	K_b [L mol^{-1}]	R^2	$X_m \times 10^4$ [mol g^{-1}]	$K \times 10^{-9}$	R^2	ΔG [kJ mol^{-1}]	Δ H [kJ mol^{-1}]	ΔS [J K^{-1} mol^{-1}]
298	11.38	17061	0.99	7.63	-5	0.99	-23.92		
308	11.05	11519	0.98	9.48	-5	0.98	-24.28		
318	10.34	10954	0.97	9.37	-5	0.97	-24.65	-12	36
328	9.75	10269	0.99	7.62	-5	0.97	-25.02		

The feasibility of the adsorption can be predicted in terms of dimensionless constant (R_L), defined by the following expression

$$R_L = \frac{1}{1+K_b C_i} \quad (18)$$

where K_b is the Langmuir binding constant and C_i is the initial concentration of arsenite.

$R_L>1$ unfavorable, $R_L=0$ Irreversible, $R_L=1$ Linear, $0<R_L<1$ Favorable [44]

The R_L values for As(III) sorption onto Fe-UTAC are lesser than unity and greater than zero at all temperatures and concentrations (Table 4), suggesting favorable adsorption process. The R_L values decrease with increase in concentration of As(III) but increase with rise in temperature indicating that As(III) sorption onto Fe-UTAC is more favorable at higher concentrations and lower temperature.

Table 4. Values of R_L for As(III) sorption on Fe-UTAC at pH 8 and different temperatures.

Conc. × 10^5 [mol L^{-1}]	Temp [K]			
	298	308	318	328
1.40	0.81	0.86	0.87	0.87
13.1	0.31	0.39	0.41	0.43
33.4	0.15	0.21	0.22	0.22
41.1	0.12	0.17	0.18	0.19

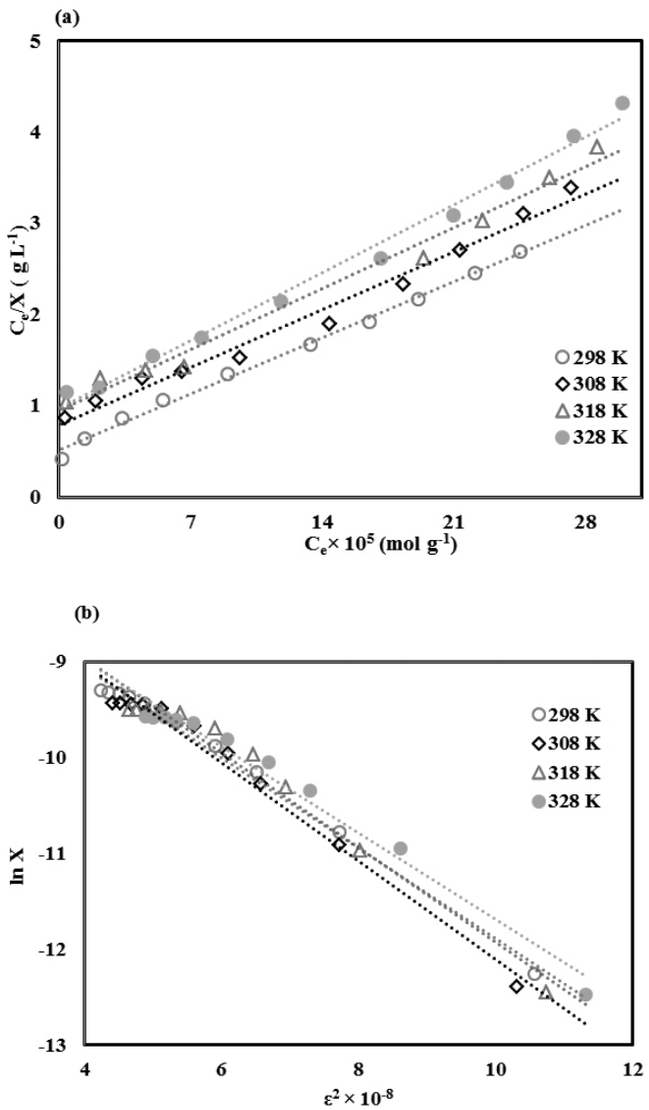

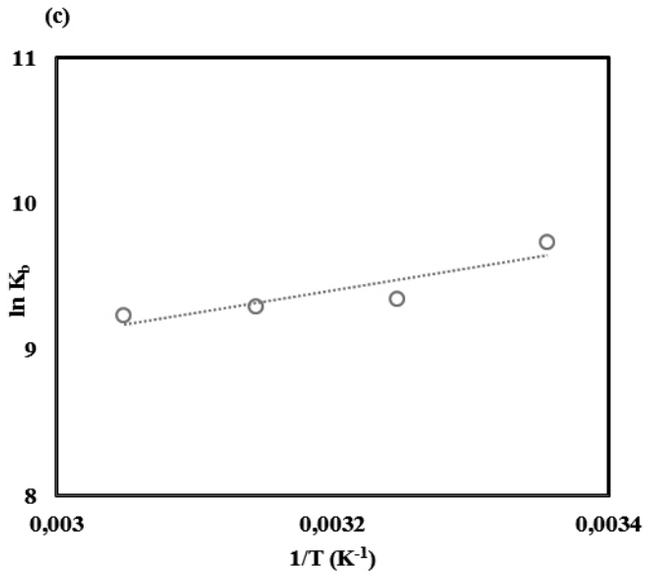

Fig. 8(a) Langmuir, (**b**) D-R and **(c)** Van't Hoff plots for the adsorption of As(III) on Fe-UTAC.

3.5.2 Dubinin- Radushkevich *(D-R) model*

The D-R model which is used to determine the energy of sorption as well as to differentiate between chemisorption and physisorption is given in its linear form as:

$$\ln X = lnX_m - K\varepsilon^2 \quad (19)$$

Where q_m (molg^{-1}) is D-R adsorption capacity and is given as follows:

$$\varepsilon = \mathrm{RT}\ln\left[1 + \left(\frac{1}{C_e}\right)\right] \quad (20)$$

The plots of ln X vs. ε^2 at different temperatures (Fig. 8b) give a linear relationship with $R^2 > 0.97$ for As(III) sorption onto Fe-UTAC. The X_m and K values calculated from the slope and intercept of the plots are given in Table 3. The sorption energy was calculated from the following mathematical expression:

$$E = \frac{1}{\sqrt{-2K}} \quad (21)$$

The values of sorption energy (E) in the range 8 - 16 kJ mol^{-1} indicate chemisorption (ion exchange mechanism) while E values below 8 kJ mol^{-1} represent physisorption [43]. In the present study, sorption energy was found to be 10 kJ mol^{-1}, which indicates that anion exchange mechanism is responsible for the sorption of arsenite onto the surface of Fe-UTAC.

3.6 Comparison of adsorption capacity

The direct comparison of the adsorption capacity of Fe-UTAC with other adsorbents is challenging due to differences in experimental conditions which are considerably counted for the variation of the adsorption capacities. However, for the sake of comparison, the values of maximum adsorption capacity (X_m) collected from the literature for various adsorbents and the one observed for the iron impregnated activated carbon in the present study are given in Table 5. The comparison of adsorption capacity indicates that adsorption capacity (mg g^{-1}) of Fe-UTAC is greater in magnitude than the adsorbents previously studied [44, 46-49, 52, 53]. Hence, Fe-UTAC is a promising material for the removal of As(III) under the prescribed conditions as compared to other adsorbents.

3.7 Thermodynamic parameters

The changes in enthalpy (ΔH), entropy (ΔS) and Gibbs free energy (ΔG) for the adsorption of As(III) on Fe-UTAC at different temperatures were determined using the following equations:

$$\ln K_b = -\frac{\Delta H}{RT} + \frac{\Delta S}{R} \quad (22)$$

$$\Delta G = \Delta H - T\Delta S \quad (23)$$

where K_b is the Langmuir constant. The ΔH and ΔS values were calculated from the slope and intercept respectively, of the plot of ln K_b vs. T^{-1} (Fig. 8c) and are tabulated in Table 3.

The negative ΔH value suggested the exothermic nature of the adsorption process as reported by Kundu and Gupta [44] for iron oxide coated cement. As can be seen from the Table 3, the decrease in ΔG value with rise of temperature shows that feasibility of adsorption decreases with the rise of temperature, which confirms the exothermic nature of the adsorption process [43]. The negative ΔG and positive ΔS values confirm the feasibility and spontaneity of the sorption process. Furthermore, the positive ΔS value showed increasing randomness during the sorption of As(III) on Fe-UTAC and also reflected the randomness at the solid/liquid interface during arsenite adsorption onto Fe-UTAC [54].

Table 5. Comparison of the adsorption capacities of different adsorbents for As(III).

Adsorbent	pH	Temp (K)	Adsorption capacity (mg g^{-1})	Reference
Iron oxide coated cement	7	300	0.69	43
Activated alumina	6.9	-	3.48	45
Iron modified bamboo charcoal	4-5	298	7.23	46
Iron oxide nanoparticle impregnated carbon nanotubes	8	298	5.25	47
Ferric ion loaded red mud	7	-	4.00	48
Magnetic wheat straw	7-9	303	3.89	51
Magnetic iron oxide nanoparticles coated on sand	7	298	0.28	52
Fe-UTAC	8	298	6.83	Present study

4. CONCLUSIONS

From the overall discussion, it is concluded that activated carbon prepared from UT by activation with phosphoric acid had a higher surface area than UT. The impregnation of the UTAC by iron oxide resulted in an increase in the adsorption capacity of the resultant Fe-UTAC. The sorption capacity of Fe-UTAC was almost three and six times larger than that of UTAC and UT respectively. The uptake of arsenite by different adsorbents followed the order; Fe-UTAC > UTAC > UT. The slight release of iron in the pH range 2 - 3 and 10 - 12 indicated that the arsenite anion is dragging iron from the Fe-UTAC to form complexes in the aqueous phase. Maximum adsorption of As(III) in the pH range 7 - 8 may be correlated with the stability of Fe-UTAC as no release of iron from Fe-UTAC was observed in this pH range. Richenberg model confirmed film diffusion to be the main rate limiting step for the removal of arsenite from aqueous solution onto Fe-UTAC. Hence the present study demonstrated that Fe-UTAC is a viable material for the treatment of arsenic containing aqueous solution.

REFERENCES

[1] Choi J, Yang JS, Park YT, Kim JO, Kim KJ, Shim YS, Kwon HH, Khan MA, Park JW, UM JG, Jeon BH. Comparison of As, Ni, Zn, Cd and Pb removals using treatment agents. *Environ. Technol.* **33,** 445-454 (2012).

[2] Ghomri F, Lahsini A, Laajeb A, Addaou A. The removal of heavy metal ions (copper, zinc, nickel and cobalt) by natural bentonite. *Larhyss J.* **12**, 37-54 (2013).

[3] Meher AK, Das S, Rayalu S, Bansiwal A. Enhanced arsenic removal from drinking water by iron-enriched aluminosilicate adsorbent prepared from fly ash. *Desalin. Water Treat.* **57**, 20944-20956 (2016).

[4] Abid M, Niazi NK, Bibi I, Murtaza G, Kunhikrishnan A, Seshadri B, Shahid M, Ali S, Bolan NS, Ok YS, Abid M, Ali F. Arsenic (V) biosorption by charred orange peel in aqueous environments. *Int J. Phytoremediat.* **18**, 442-449 (2016).

[5] De Oliveira LK, Melo CA, Goveia D, Lobo FA, Hernandez, MAA, Fraceto LF, Rosa AH. Adsorption/desorption of arsenic by tropical peat: influence of organic matter, iron and aluminium. *Environ. Technol.* **36**, 149-59 (2015).

[6] Lunge S, Singh S, Sinha A. Magnetic iron oxide (Fe_3O_4) nano particles from tea waste for arsenic removal. *J. Magn. Magn. Mater.* **356** 21–31 (2014).

[7] Ansari R, Sadegh M. Application of activated carbon for removal of arsenic ions from aqueous solutions. *E-J Chem.* **4**, 103-108 (2007).

[8] Hossain I, Anjum N, Tasnim T. Removal of arsenic from contaminated water utilizing tea waste. *Int. J. Environ. Sci. Technol.* **13**, 843–848 (2016).

[9] Polowczyk I, Bastrzyk A, Ulatowska J, Szczałba E, Koźlecki T, Sadowski Z. Influence of pH on arsenic (III) removal by fly ash. *Separ. Sci. Technol.* (2016). 10.1080/01496395.2016.1163610.

[10] Podder MS, Majumder CB. Sequestering of As(III) and As(V) from wastewater using a novel neem leaves/$MnFe_2O_4$ composite biosorbent. *Inter. J. Phytoremediat.* **18**, 1237-1257 (2016).

[11] Salameh Y, Al-Muhtaseb AH, Mousa H, Walker GM, Ahmad MNM. Characterization of adsorption of aqueous arsenite and arsenate onto charred dolomite in microcolumn systems. *Environ. Technol.* **35**, 3029-3040 (2014).

[12] Hamayun M, Mahmood T, Naeem A, Mustafa S, Waseem M. Equilibrium and kinetics studies of arsenate adsorption by $FePO_4$. *Chemosphere* **99**, 207–215 (2014).

[13] Beduk F. Superparamagnetic nanomaterial Fe_3O_4-TiO_2 for the removal of As(V) and As(III) from aqueous solutions. *Environ. Technol.* **37**, 1790-1801 (2016).

[14] Sanchez J, Toledo L, Bernabe LR, Rivera N , Munoz E. Water-soluble cationic cellulose coupled to a ultrafiltration membrane for the removal of arsenic and chromium. *J. Chil. Chem. Soc.* **58**, 1986-1990 (2013).

[15] Dong L, Liu W, Jiang R, Wang Z. Study on the adsorption mechanism of activated carbon removing low concentrations of heavy metals. *Desalin. Water Treat.* **57**, 7812-7822 (2016).

[16] Shakoor MB, Niazi NK, Bibi I, Murtaza G, Kunhikrishnan A, Seshadri B, Shahid M, Ali S. Bolan NS, Ok YS, Abid M, Ali F. Remediation of arsenic-contaminated water using agricultural wastes as biosorbents. *Crit. Rev. Env. Sci. Technol.* **46**, 467-499 (2016).

[17] Prahas D, Kartika Y, Indraswati N, Ismadji S. Activated carbon from jackfruit peel waste by H_3PO_4 chemical activation: Pore structure and surface chemistry characterization. *Chem. Eng. J.* **140**, 32-42 (2008).

[18] Gomez-Serrano V, Cuerda-Correa EM, Fernandez-Gonzalez, MC, Franco MFA, Garcıa AM. Preparation of activated carbons from chestnut wood by phosphoric acid-chemical activation. Study of microporosity and fractal dimension. *Mater. Lett.* **59**, 846-853 (2005).

[19] Bahri MA, Calvo L, Gilarranz MA, Rodriguez JJ. Activated carbon from grape seeds upon chemical activation with phosphoric acid: Application to the adsorption of diuron from water. *Chem. Eng. J.* **203**, 348-356 (2012).

[20] Gupta VK, Pathania D, Sharma S. Adsorptive remediation of Cu(II) and Ni(II) by microwave assisted H_3PO_4 activated carbon. *Arab. J. Chem.* (2013) 10.1016/j.arabjc.2013.11.006.
[21] Dieme MM, Villot A, Gerente C, Andres Y, Diop SN, Diawara CK. Sustainable conversion of agriculture wastes into activated carbons energy balance and arsenic removal from water. *Environ. technol.* 10.1080/09593330.2016.1193225 (2016).
[22] Yu MR, Chang YY, Yang JK. Application of activated carbon impregnated with metal oxides to the treatment of multi contaminants. *Environ. technol.* **33**, 1553-1559 (2012).
[23] Gundogdu A, Duran C, Senturk HB, Soylak M, Ozdes D, Serencam H, Imamoglu M. Adsorption of phenol from aqueous solution on a low-cost activated carbon produced from tea industry waste: Equilibrium, kinetic, and thermodynamic study. *J. Chem. Eng. Data* **57**, 2733-2743 (2012).
[24] Mayakaduwa SS, Vithanage M, Karunarathna A, Mohan D, Ok YS. Interface interactions between insecticide carbofuran and tea waste biochars produced at different pyrolysis temperatures. *Chem. Spec. Bioavailab.* **28**, 110-118 (2016).
[25] Akar E, Altinisik A, Seki Y. Using of activated carbon produced from spent tea leaves for the removal of malachite green from aqueous solution. *Ecol. Eng.* **52**, 19-27 (2013).
[26] Panneerselvam P, Morad N, Tan KA. Magnetic nanoparticle (Fe_3O_4) impregnated onto tea waste for the removal of nickel(II) from aqueous solution. *J. Hazard. Mater.* **186**, 160 – 168 (2011).
[27] Shamsuddin MS, Yusoff NRN, Sulaiman MA. Synthesis and characterization of activated carbon produced from kenaf core fiber using H_3PO_4 activation. *Procedia Chem.* **19**, 558 – 565 (2016).
[28] Rajapaksha AU, Vithanage M, Zhang M, Ahmad M, Mohan D, Chang SX, Ok YS. Pyrolysis condition affected sulfamethazine sorption by tea waste biochars. *Bioresour. Technol.* **166**, 303-308 (2014).
[29] Nethaji S, Sivasamy A, Mandal AB. Preparation and characterization of corn cob activated carbon coated with nano-sized magnetite particles for the removal of Cr(VI). *Bioresour. Technol.* **134**, 94-100 (2013).
[30] Sulyman M, Namiesnik J, Gierak A. Utilization of new activated carbon derived from oak leaves for removal of crystal violet from aqueous solution. *Pol. J. Environ. Stud.* **23**, 2223-2232 (2014).
[31] Soleimani M, Kaghazchi T. Agricultural waste conversion to activated carbon by chemical activation with phosphoric acid. *Chem. Eng. Technol.* **30**, 649-654 (2007).
[32] Maiti A, Agarwal V, De S, Basu JK. Removal of As(V) using iron oxide impregnated carbon prepared from tamarind hull. *J. Environ. Sci. Heal. A* **45**, 1207 – 1216 (2010).
[33] Mohan D, Sarswat A, Singh VK, Franco MA, Jr CUP. Development of magnetic activated carbon from almond shells for trinitrophenol removal from water. *Chem. Eng. J.* **172**, 1111– 1125 (2011).
[34] Liu Z, Zhang FS, Sasai R. Arsenate removal from water using Fe_3O_4-loaded activated carbon prepared from waste biomass. *Chem. Eng. J.* **160**, 57 – 62 (2010).
[35] Krejcova A, Tomas C. The determination of boron in tea and coffee by ICP–AES method. Food Chem. **82,** 303–308 (2003).
[36] Malkoc E, Nuhoglu Y. Removal of Ni(II) ions from aqueous solutions using waste of tea factory: Adsorption on a fixed-bed column. *J. Hazard. Mater.* **135**, 328-336 (2006).
[37] Marin MO, Gonzalez CF, Garcia AM, Serrano VG. Preparation of activated carbon from cherry stones by physical activation in air. Influence of the chemical carbonization with H_2SO_4. *J. Anal. Appl. Pyrolysis* **94**, 131–137 (2012).
[38] Liou TH. Development of mesoporous structure and high adsorption capacity of biomass-based activated carbon by phosphoric acid and zinc chloride activation. *Chem. Eng. J.* **158**, 129–142 (2010).
[39] Karaagac O, Kockar H, Beyaz S. A Simple way to synthesize superparamagnetic iron oxide nanoparticles in air atmosphere: Iron ion concentration effect. *IEEE Trans Magn.* **46**, 3978 – 3983 (2010).
[40] Gupta VK, Nayak A. Cadmium removal and recovery from aqueous solutions by novel adsorbents prepared from orange peel and Fe_2O_3 nanoparticles. *Chem. Eng. J.* **180**, 81- 90 (2012).
[41] Podder MS, Majumder CB. Studies on the removal of As(III) and As(V) through their adsorption onto granular activated carbon/$MnFe_2O_4$ composite: isotherm studies and error analysis. *Compos. Interf.* **23**, 327-372 (2016).
[42] Mahmood T, Din SU, Naeem A, Mustafa S, Waseem M, Hamayun M. Adsorption of arsenate from aqueous solution on binary mixed oxide of iron and silicon. *Chem. Eng. J.* **192**, 90 – 98 (2012).
[43] Ranjan D, Talat M, Hasan SH. Biosorption of arsenic from aqueous solution using agricultural residue rice polish. *J. Hazard. Mater.* **166**, 1050 – 1059 (2009).
[44] Kundu S, Gupta AK. Adsorption characteristics of As(III) from aqueous solution on iron oxide coated cement (IOCC). *J. Hazard. Mater.* **142**, 97-104 (2007).
[45] Maji SK, Pal A, Pal T, Adak A. Adsorption thermodynamics of arsenic on laterite soil. *J. Surface Sci. Technol.* **22**, 161-176 (2007).
[46] Lin TF, Wu JK. Adsorption of arsenite and arsenate within activated alumina grains: Equilibrium and kinetics. *Wat. Res.* **35**, 2049 – 2057 (2001).
[47] Liu X, Ao H, Xiong X, Xiao J, Liu J. Arsenic removal from water by iron-modified bamboo charcoal. *Wat. Air Soil Pollut.* **223**, 1033-1044 (2012).
[48] Tawabini BS, Al-Khaldi SFA, Khaled MM, Atieh MA. Removal of arsenic from water by iron oxide nanoparticles impregnated on carbon nanotubes. *J. Environ. Sci. Heal. A* **46**, 215-223 (2011).
[49] Kocabas ZO, Yurum Y. Kinetic Modeling of arsenic removal from water by ferric ion loaded Red Mud. *Sep. Sci. Technol.* **46**, 2380-2390 (2011).
[50] Biswas BK, Junichi I, Katsutoshi I, Nath GK, Hiroyuki H, Keisuke O, Hidetaka K. Adsorptive removal of As(V) and As(III) from water by a Zr(IV)-loaded orange waste gel. *J. Hazard. Mater.* **154**, 1066-1074 (2008).
[51] Ngantcha TA, Vaughan R, Reed BE. Modeling As(III) and As(V) removal by an iron oxide impregnated activated carbon in a binary adsorbate system. *Sep. Sci. Technol.* **46**, 1419-1429 (2011).
[52] Tian Y, Wu M, Lin X, Huang P, Huang Y. Synthesis of magnetic wheat straw for arsenic adsorption. *J. Hazard. Mater.* **193**, 10-16 (2011).
[53] Afzali D, Rouhani M, Fathirad F, Shamspur T, Mostafavi A. Nano iron oxide coated on sand as a new sorbent for removal of arsenic from drinking water. *Desalin. Water Treat.* **57**, 13030-13037 (2016).
[54] Das B, Devi RR, Umlong IM, Borah K, Banerjee S, Talukdar AK. Arsenic (III) adsorption on iron acetate coated activated alumina: Thermodynamic, kinetics and equilibrium approach. *J. Environ. Heal. Sci. Eng.* **11**, 1-10 (2013).